Chapter 2

Experimental Apparatus and Diagnostics

2.1 The Basil Experimental Apparatus

The Basil experiment is a linear magnetised plasma produced by rf excitation of helicon waves. The magnetic field is produced by 14 electromagnets arranged to give a uniform magnetic field approximately 1.4m long. The rf antenna is installed on the outside of the cylindrical glass vacuum vessel at the midpoint of the magnetic field (see figure 2.1).

This chapter describes the apparatus, diagnostics and the control and data acquisition system in detail. The apparatus can be divided into three main sections: the vacuum system, the static magnetic field and the rf system. Subsections of the rf section describe the antennas, the matching network, rf power and loading measurements and the rf power splitter. The diagnostics are divided into two sections - the Langmuir probes for measuring plasma characteristics and the magnetic probes for measuring wavefields. Finally, the

control and data acquisition system is described.

2.1.1 The Vacuum System

The overall length of the vacuum system is approximately 2 metres. Most of this length consists of two Pyrex tubes (outside diameter 50mm) with a probe chamber 450mm from one end of the field coils (the probe chamber joins the two Pyrex tubes, figure 2.1). The probe chamber, which is supported by the field coils, allows a Langmuir probe and a three component magnetic probe to be moved radially in the plasma. Outside the ends of the field coils the Pyrex tubes are supported by stainless steel stands that allow end plates (aluminium or quartz windows) to be fitted.

The support furthest from the vacuum pumps has Alcatel Pirani and Penning vacuum gauges while at the other end support there is a capacitance diaphragm vacuum gauge (Vacuum General Inc. CMH series). To stop condensation when bringing the system up to atmospheric pressure there is a nitrogen feed at the end support furthest from the vacuum pumps. The aluminium end plate for the end support furthest from the vacuum pumps has an O-ring sealed vacuum feed for a hooked probe which can be drawn along the axis of the Pyrex tube.

The support at the vacuum pump end has a gas feed from a MKS mass flow controller which maintains a stable filling pressure. On the high pressure side of the mass flow controller a set of valves allow easy changing of gases with no need to let air into unused gas lines, thus avoiding the necessity of purging the lines with every gas change.

The Alcatel vacuum gauges are used as a backup to the capacitance diaphragm gauge and as an indicator of when the base pressure has been reached (approximately 1×10^{-5}

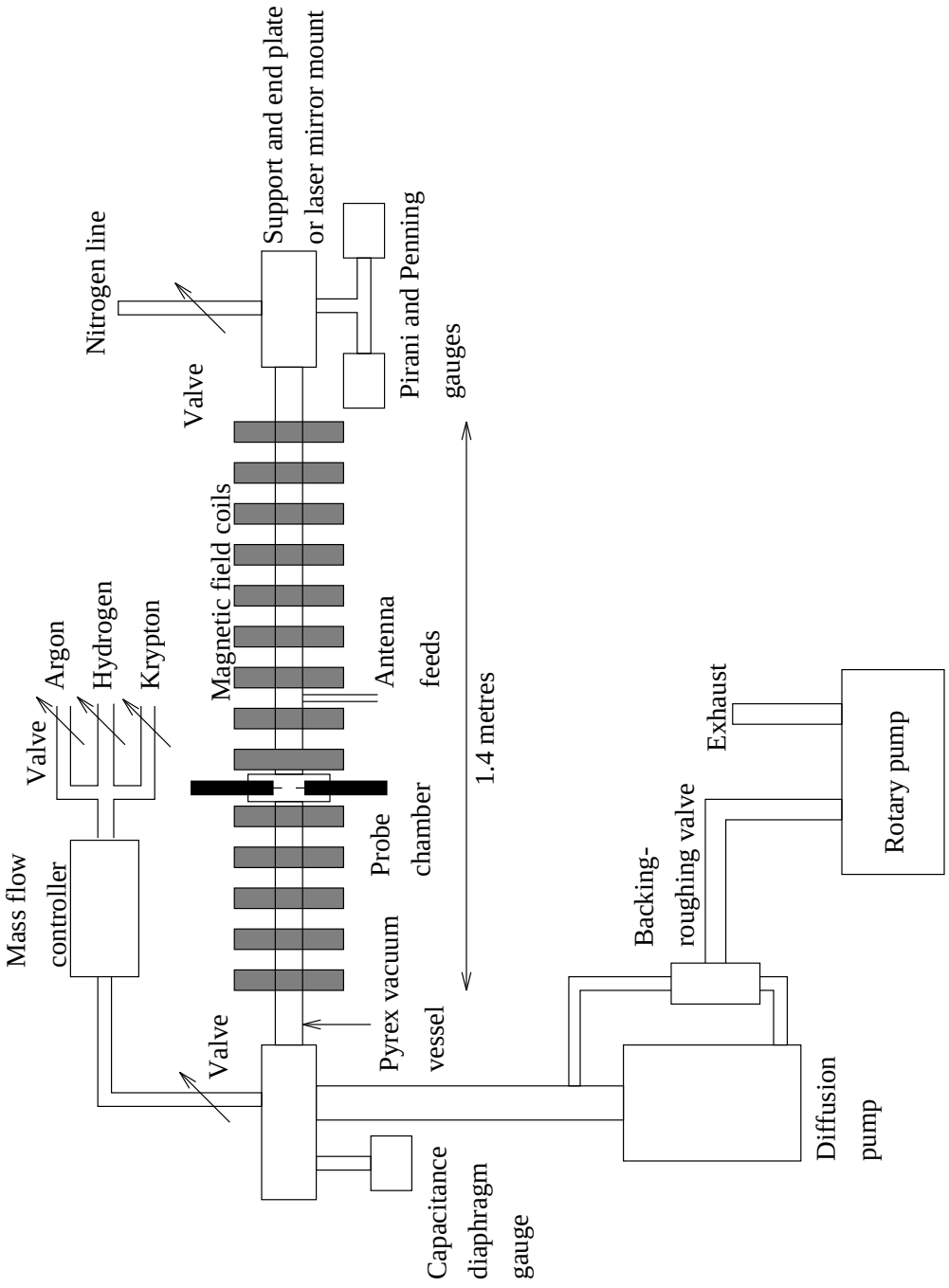

Figure 2.1: *Vacuum system and gas feeds.*

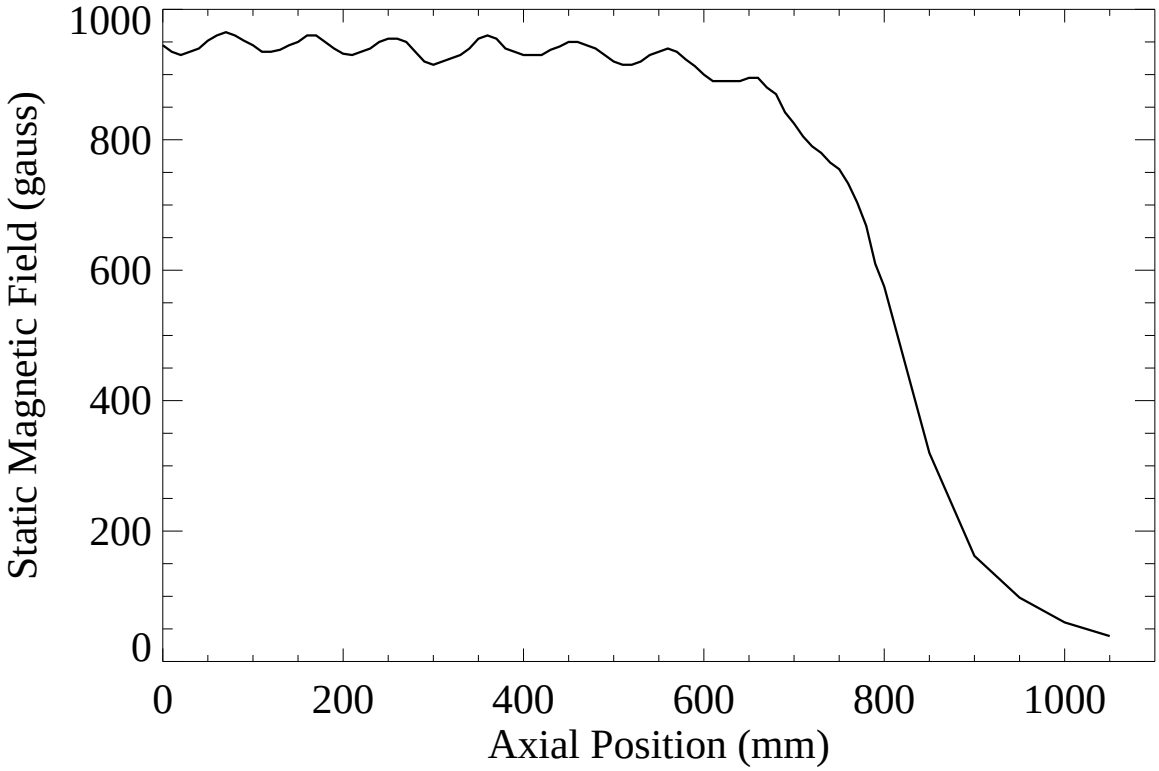

Figure 2.2: *The static magnetic field on axis as a function of axial position*

Torr). Once the base pressure has been reached the capacitance diaphragm gauge is zeroed and all subsequent filling pressure measurements are made by this gauge. The filling pressure is then held constant by adjusting the flow of gas. The capacitance diaphragm gauge has to be regularly zeroed because of drifts caused by temperature fluctuations.

2.1.2 The Magnetic Field

The applied static magnetic field is produced by 14 water cooled co-axially mounted magnetic field coils powered by a 160 amp, 1 ohm power supply. The resultant static field is approximately 1.2 metres long with a ripple of less than 5% and a maximum strength of 0.2 Tesla. A plot of the longitudinal field along half the vacuum vessel as measured

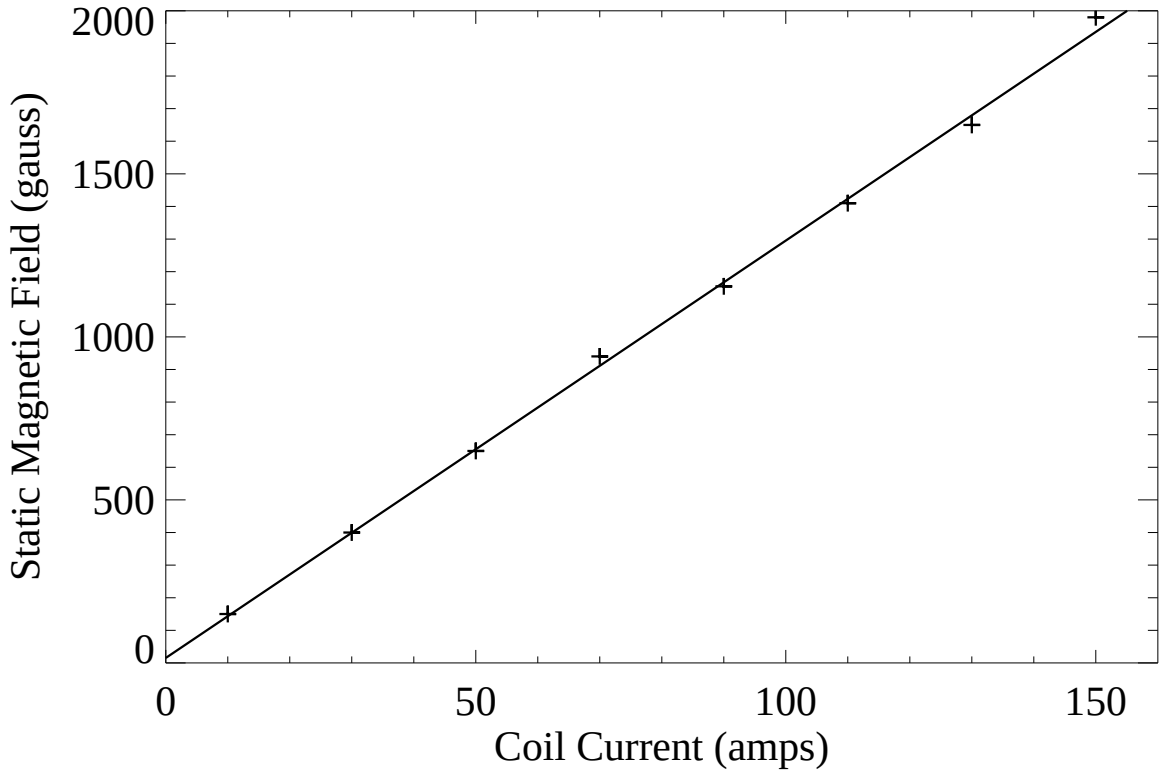

Figure 2.3: *The static magnetic field on axis as a function of current*

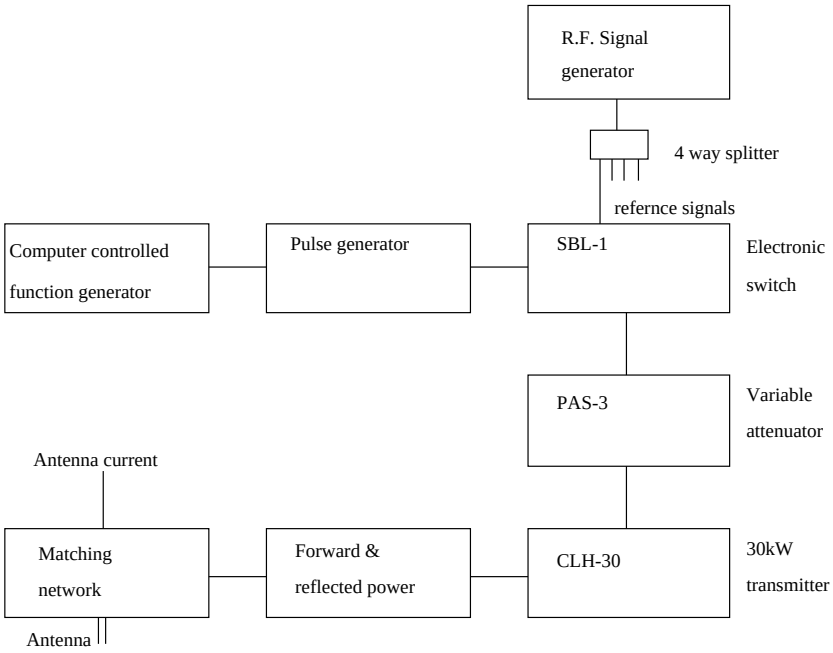

Figure 2.4: *The rf system.*

on axis is shown in figure 2.2 (current 70 amps, antenna feeders are at position 0mm) and figure 2.3 is a plot of the field strength versus coil current at the position 550mm in figure 2.2.

2.2 R.F. System

The Basil experiment takes advantage of the availability of a 30kW transmitter (AWA, CLH-30) used on the H-1 Heliac experiment. While this is more than twice the power required for Basil it has the useful consequence that the transmitters tolerate large impedance mismatches at the Basil operating powers, making tuning much easier. Since the experiment is run in a pulsed mode of operation a gated rf signal, the amplitude of which can be varied is needed to drive the transmitter, while a signal of constant amplitude is needed

as a reference for making rf measurements. This is achieved by using a continuous rf signal which is split four ways. One of these signals is then chopped by a mini-circuits frequency mixer (SBL-1) made to act as a high speed electronic switch. The level of the signal is then adjusted with a mini-circuits (PAS-1) electronic attenuator which has an approximate range of 2dB to 25dB. this signal is then used to drive the transmitter while the three remaining signals are used as references.

The rf power from the transmitter is then fed to the experiment by a 50Ω semi-rigid coaxial cable (RG 231). Signals proportional to the forward and reflected power are obtained before the matching network by the method described in Section 2.2.3. The antenna is incorporated into a π-network for impedance matching and this is described in Section 2.2.2 . For antenna loading measurements and as a tuning indicator the current in the antenna is measured with a step down current transformer.

2.2.1 Antennas

To determine the important factors involved in wave launching, experiments with three types of antennas have been undertaken.

1. *Double Saddle Coil Antenna*

   The double saddle coil antenna consists of two current loops on either side of the plasma (outside the vacuum tube) with the currents circulating in phase. This is achieved by constructing the antenna from one length of heavy copper wire. To ensure the current is the same in the two loops the total length of wire used in constructing the antenna is much less than one wavelength of the rf signal driving

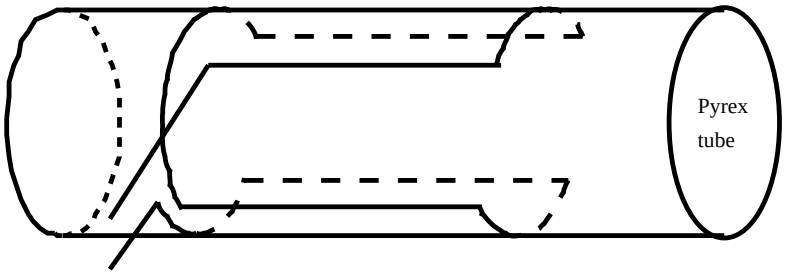

Figure 2.5: *Double saddle coil antenna.*

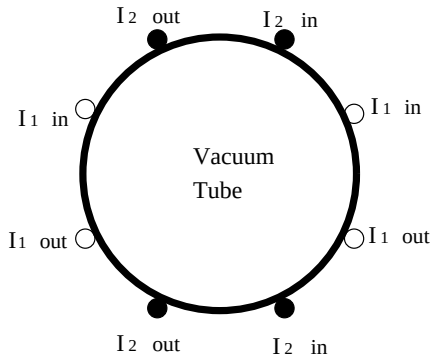

Figure 2.6: *A cross section of the two phased double saddle coil antennas. The magnitude of the currents in the two pairs are equal and the phase can be varied. This antenna consists of two orthogonal double saddle coil antennas.*

it. Helicon source plasma processing machines generally use this type of antenna configuration.

2. *Phased Array of Orthogonal Double Saddle Coil Antennas*

   To have some control over the magnitude of the $m = +1$ and $m = -1$ components of the helicon wave that is launched, two double saddle coil antennas are positioned 90^o azimuthally from each other and the phase of the currents are varied while their magnitudes are held the same. The antenna is constructed such that the longitudinal components of the antenna are evenly spaced around the tube and the wire is

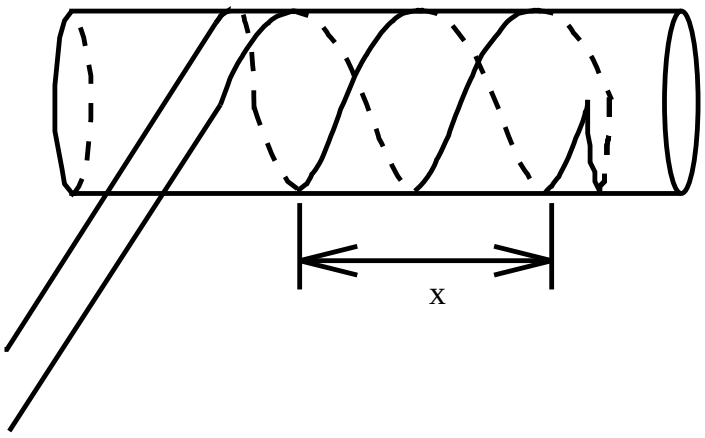

Figure 2.7: *Helically wound antenna.*

embedded in Delrin to reduce arcing.

The phase of the currents are varied by using an rf power splitter to obtain signals for each pair of loops and delaying the signals with a simple length of delay line. One of the problems with this antenna is the coupling of the two pairs of loops due to their mutual inductance. This is eliminated by putting the antenna in series with a 1:1 transformer wound in a sense that its mutual inductance cancels that of the antennas. By careful adjustment, the cross talk induced in one antenna by the other, in the absence of plasma can be reduced to 5%. The current in each pair is monitored with current transformers and each pair of loops require a matching network.

3. *Helical Antenna*

The helical antenna consists of two helical windings wound around the outside of the vacuum vessel, each azimuthally 180^0 displaced. The current in each winding is in the opposite direction to each other. This antenna is easily constructed with

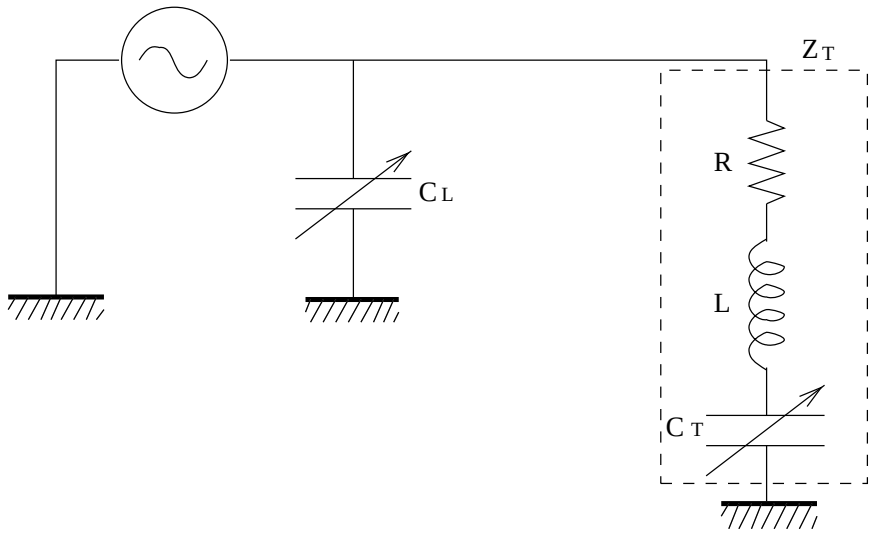

2.8: *Circuit diagram of a π-network where the antenna is represented by R and L.*

one length of heavy copper wire, with the two windings joined by a half loop at one end. Again, the total length of wire used in constructing the antenna is much less than one wavelength of the rf signal used to drive it. The helical antenna has a higher selectivity of parallel wavelength than the double saddle coil antenna, thus decreasing its useful wavelength range. For the Basil experiment the length chosen is 18cm and the total length of the antenna is one and a half wavelengths.

2.2.2 Matching Network

To ensure that the transmission line from the rf transmitter is terminated at its characteristic impedance the antenna is incorporated into a π-network, where the antenna is the inductor as shown in figure 2.8. When there is no plasma the resistance R is the electrical resistance of the antenna. Once a plasma is produced the resistance will increase.

For design purposes an estimate of the load capacitance and tune capacitance (C_L

and C_T, respectively) for an approximate loading or radiation resistance and antenna inductance is useful. Taking the tune arm of the network which includes the antenna, the impedance is given by

$$Z_T = j\omega L + \frac{1}{j\omega C_T} + R : \tag{2.1}$$

Now assume that the tune capacitance does not completely cancel out the antenna inductance so that the tune arm will have a net inductive impedance which can be balanced by the load capacitance. Thus equation 2.1 can be written

$$Z_T = jL^* + R \tag{2.2}$$

where

$$L^* = L\omega - \frac{1}{\omega C_T} \tag{2.3}$$

The admittance of the tune arm Y_T is

$$Y_T = \frac{R}{R^2 + L^{*2}} - \frac{L^* j}{R^2 + L^{*2}} \tag{2.4}$$

The admittance of the load arm Y_L is

$$Y_L = j\omega C_L \tag{2.5}$$

The total admittance of the circuit is

$$Y_{total} = Y_T + Y_L \tag{2.6}$$

If the tune arm is at resonance with the load capacitor then the total conductance will equal the inverse of the line impedance Z when matched, and the susceptance of the tune and load arms will cancel. This gives the following equations respectively

$$L^{*2} = R(Z - R) \tag{2.7}$$

$$C_L = \frac{L^*}{RZ\omega} \tag{2.8}$$

In this experiment it is possible to make the assumption that $Z \gg R$, thus equation 2.7 gives

$$L^* = \sqrt{RZ} \tag{2.9}$$

Combining equations 2.8 and 2.9 gives

$$C_L = \frac{1}{\omega\sqrt{RZ}} \tag{2.10}$$

Expanding L^* in equation 2.7 gives

$$C_T = \frac{1}{\omega^2 L - \omega\sqrt{RZ}} \tag{2.11}$$

Taking the typical case: f =7MHz, $\omega = 4.4 \times 10^7$rad sec^{-1}, $L = 0.5\mu$H , $R = 1\Omega$, $Z = 50\Omega$. The tune and load capacitances are found from Equations 2.11 and 2.10 to be: $C_T = 1500$pF, and $C_L = 3200$pF.

In this experiment the matching box consists of two variable vacuum capacitors with a range of 1000pF for the tune and load capacitances. Fixed value high voltage ceramic

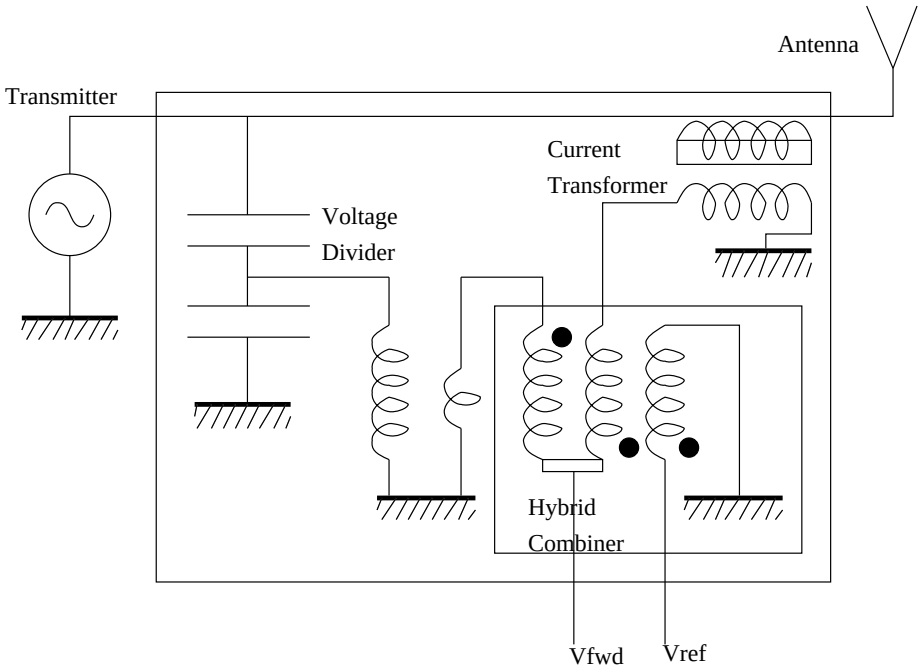

Figure 2.9: *The circuit used in determining the power by measuring the forward and reflected voltages.*

capacitors (1000pF, 500pF and 100pF) can be put inf parallel with these to reach the desired values.

2.2.3 RF Power Measurements

Measuring high power rf is not easily done but very important for determining how much power is being coupled into the plasma and thus the loading or radiation resistance of the antenna. The antenna radiation resistance is the principle measure of the efficiency of an antenna. By using a current step down transformer and a capacitive divider (see figure 2.9), which is stepped down with a voltage transformer, the line current I and voltage V can be measured.

The voltage and current on the line are given in terms of the forward and reflected

voltage and current by the following expression.

$$V = V_{fwd} + V_{ref} \tag{2.12}$$

$$I = I_{fwd} + I_{ref} = \frac{V_{fwd} - V_{ref}}{Z_O} \tag{2.13}$$

where the forward and reflected powers are

$$P_{fwd} = \frac{(C\,V_{fwd})^2}{Z_O} \tag{2.14}$$

$$P_{ref} = \frac{(C\,V_{ref})^2}{Z_O} \tag{2.15}$$

and Z_O is the characteristic impedance of the line and C is a calibration factor.

From Equations 2.12 and 2.13 the forward and reflected line voltages are

$$V_{fwd} = \frac{V + Z_O I}{2} \tag{2.16}$$

$$V_{ref} = \frac{V - Z_O I}{2} \tag{2.17}$$

If the output of the voltage divider, V, and current transformer, I, are fed into a hybrid combiner as in figure 2.9, then from Equations 2.13, 2.16, and 2.17 the outputs will be proportional to the forward and reflected voltages. For the Basil experiment two power measuring circuits are used and the calibration factors are 2070 and 4690 for boxes 1 and 2.

Number 1	Number 2	Number 3
201	100	90

Table 2.1: *Calibration factors D, of the current transformers at 7MHz.*

The line diagnostic can be operated at 10kW CW [12]. From figure 2.9 it can be seen that the high power rating is achieved by using a capacitive divider for the voltage measurements, rather than cascaded voltage transformers, so that overheating of ferrite transformer coils is avoided.

2.2.4 Antenna Loading Measurements

The dissipation of power into the plasma is seen as a resistive loading of the antenna. The resistive loading can be calculated from

$$I_{ant}^2 R_{total} = P_{fwd} - P_{ref} \tag{2.18}$$

As already mentioned the resistive loading of the antenna is due to the plasma and the electrical resistance of the material that the antenna is made of.

$$R_{total} = R_{ant} + R_{plasma} \tag{2.19}$$

The electrical resistance of the antenna can be determined by measuring the antenna loading with no plasma. This is achieved by reducing the power so that a plasma does not form. The current in the antenna is measured with a current step down transformer. Because of the high voltages in the tuned matching network the current transformer needs

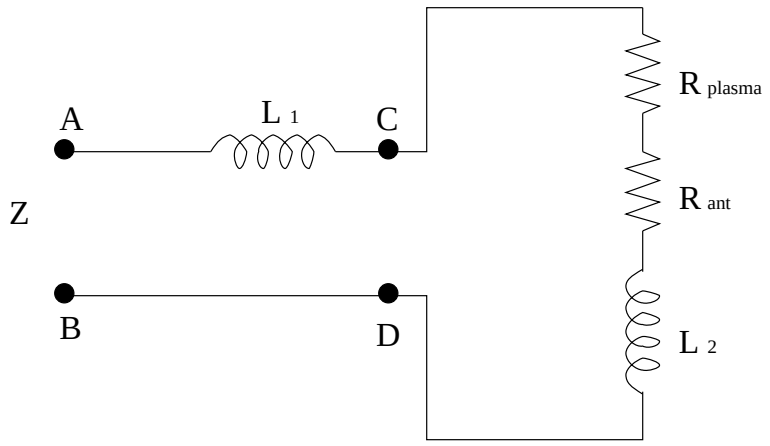

Figure 2.10: *The equivalent circuit of the antenna and its feeders.*

to be electro statically shielded. In the Basil experiment 3 different current transformers are used and their calibration factors are given in table 2.1 ($I_{ant} = DV_{out}$, where V_{out} is the signal from current transformer).

Finally, once the electrical resistance of the antenna is known, by measuring the power into the matching network and current in the antenna the load due to the plasma can be calculated from

$$R_{plasma} = \frac{P_{fwd} - P_{ref}}{I^2_{antrms}} - R_{ant} \tag{2.20}$$

As the antenna is at the end of a pair of 30cm long parallel feeders, consideration must be given to the possibility of these feeders acting as transmission lines and thus transforming the measured loading. The equivalence circuit of the antenna is shown in figure 2.10, where L_1 is the inductance of the feeders, L_2 is the inductance of the antenna and R_{plasma} and R_{ant} are the resistances due to the plasma and antenna respectively.

The inductances were measured by forming a resonant circuit using capacitors with known values. Hence L_1 was determined by placing a short at CD and measuring the

Antenna	$L_1(\mu H)$	$L_2(\mu H)$
Double saddle coil	0.42	0.50
Helical	0.40	0.61

Table 2.2: *The inductances of the antennas and their feeders.*

	Resistor at CD		Resistor at AB	
$R_{test}\Omega$	$R_{meas.}$	$R_{calc.}$	$R_{meas.}$	$R_{calc.}$
6.8 K	0.32	0.28	0.46	0.47
4.3 K	0.39	0.33	0.62	0.60
2.4 K	0.60	0.49	0.97	1.0
1.0 K	1.0	0.90	2.1	2.2
390	2.3	2.0	4.9	5.2
100	7.9	6.9	15.9	16.2

Table 2.3: *Comparisons of measured and theoretical loading for the helical antenna.*

	Resistor at CD		Resistor at AB	
$R_{test}\Omega$	$R_{meas.}$	$R_{calc.}$	$R_{meas.}$	$R_{calc.}$
6.8 K	0.28	0.25	0.41	0.42
4.3 K	0.32	0.28	0.53	0.52
2.4 K	0.44	0.39	0.86	0.88
1.0 K	0.78	0.66	1.8	1.8
511	1.4	1.1	3.0	3.3
100	5.7	4.7	14.0	14.1

Table 2.4: *Comparisons of measured and theoretical loading for the double saddle coil antenna.*

resonant frequency with a range of capacitors placed across AB, while L_2 was found by similarly measuring the combined inductance $L_1 + L_2$ and subtracting L_1.

For the case of the feeders of the Basil antennas (two parallel conductors) the characteristic impedance is given by [35]

$$Z_o = 276 \log_{10} \left(\frac{s}{2a} \sqrt{\left(\frac{s}{2a}\right)^2 - 1} \right) \Omega \tag{2.21}$$

s is the separation of the centers of the parallel conductors $\approx$ 30mm, and a is the radius of the conductors $\approx$ 3.4mm. For the Basil feeders $Z_0 \approx 330\Omega$.

The absence of transmission line effects was confirmed in two ways. First a clip on current probe was used to measure the current along the length of the feeders and no significant variation in amplitude was detected. Secondly, the measurement of the inductors over a wide range of resonating capacitors (with a range of resonant frequencies from 6MHz to 50MHz) showed no systematic variation as would be expected if the feeders were acting as a transmission line. The measured inductances L_1 and L_2 for the double saddle coil and helical antennas are shown in table 2.2.

Due to the difficulty in calibrating current transformers and power measurements a test was performed to ensure the measurements of the loading are correct. By placing resistors of known values at AB and CD (see figure 2.10) it is possible to calculate a theoretical value for the loading, which can then be compared to actual measurements with the resistors in place. Metal filament resistors with a low inductance and a minimum power rating of 2 watts were used, and the power was kept close to, but less than, 1 kW so that the resistors were not damaged, and the antenna current for a vacuum tune did not

get excessively high.

For the case of a resistor placed across CD, the impedance at AB is given by

$$Z = j\omega L_1 + \frac{R_L R_V + j\omega L_2 R_L}{R_L + R_V + j\omega L_2} \tag{2.22}$$

When a resistor is placed across AB, the impedance at AB is

$$Z = \frac{R_L R_V + j\omega L_{12} R_L}{R_L + R_V + j\omega L_{12}} \tag{2.23}$$

where R_L is the test resistor, R_V is the vacuum resistance and L_{12} is $L_1 + L_2$.

When the matching network is tuned the measured loading will be the real part of the impedance. To make comparisons between the measured results and the theoretical values determined from equations 2.22 and 2.23 the vacuum resistance must be found. This is easily done by taking a measurement with no resistor. Comparisons of measured loading values, determined using known resistances at AB and CD, with calculated loading values from equations 2.22 and 2.23 are shown in tables 2.3 and 2.4. The good agreement confirms that the current and power calibrations are accurate and that the loading calculations are reliable. The vacuum resistance for both the double saddle coil and helical antennas was measured to be 0.18Ω indicating most of the losses are in the matching network..

In this thesis comparisons are made of the measured antenna loading with theoretically calculated radiation resistance.

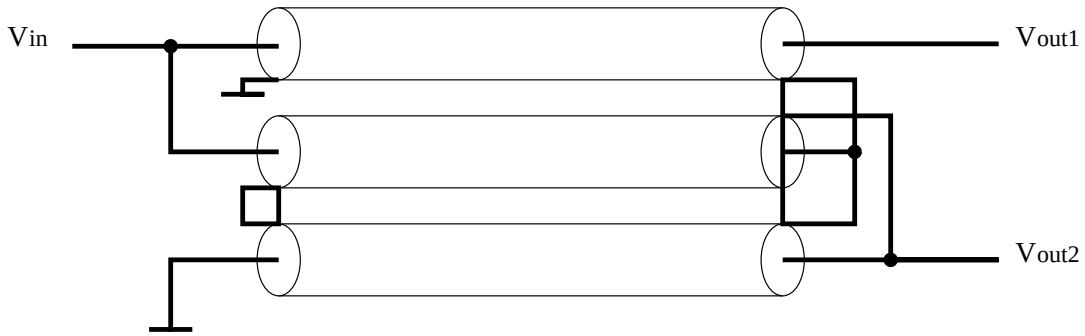

Figure 2.11: *Circuit of the power splitter.*

2.2.5 Power Splitter

The phased double saddle coil antenna requires two rf signal sources where the phase between the signals can be varied. This is done by using a high power splitter to divide the signal from the transmitter and then adjustment of the phase difference between the signals with delay cables. The power splitter used is an impedance transforming Guanella Balun [57, 11].

The circuit diagram of the power splitter in figure 2.11 shows that it consists of three transmission lines. Because of the high power which has to be split, each transmission line is wound on two 60mm outer diameter toroidal ferrites (Amidon FT240, μ=850), which reduces insertion losses and give good results over the frequency range 4-40MHz.

An analysis of the power splitter [66, 11] gives the following input to output impedance transformation and characteristic impedance

$$Z_{in} = 4Z_{out}/9 \tag{2.24}$$

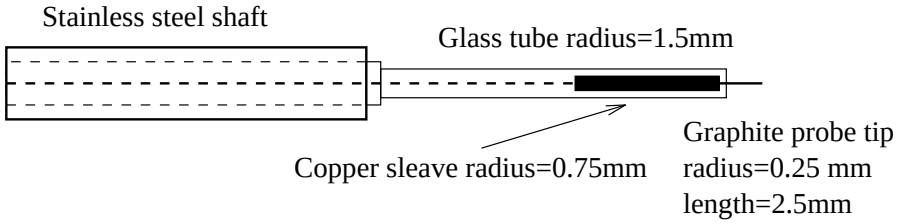

Figure 2.12: *Radial Langmuir probe design.*

$$Z_{in} = \sqrt{Z_{in} Z_{out}} \tag{2.25}$$

Thus, by constructing the power splitter with 75Ω RG59 cable, the input impedance is approximately 50Ω, which matches the transmission line from the transmitter, and the output impedance is 113Ω. Tests were performed by terminating the outputs in 100Ω and the output powers were found to be within 10%.

2.3 Langmuir Probes

In Basil two Langmuir probes are used to obtain the density and temperature of the plasma. Located 30cm from the antenna feeders on the pump side of the antenna is a radial Langmuir probe inserted via a probe chamber, which allows a break in the glass vacuum vessel. As this is the easiest site for insertion, different probe designs were tried at this location, and the final probe design includes a carbon probe tip and some filter circuitry to reduce rf effects. The hooked Langmuir probe is inserted from the end of the vacuum vessel with an O-ring seal which allows the probe to be drawn along the axis of the discharge. The design of this probe required a thin eighth inch stainless steel

probe shaft 0.4m long which limited the probe to a simple tungsten probe tip with no rf compensation.

While single Langmuir probe data requires careful interpretation the simplicity and versatility of the probe makes it ideal for Basil, where access is limited and plasma dimension are small. The high densities also render other probe methods technically difficult or expensive. Attempts to use microwave interferometry by Zhu [112] where unsuccessful as the large radial density gradient guided the waves around the high density core. In the following sections the problems associated with using Langmuir probes in high density, rf-produced, magnetised plasmas are discussed and the analytic techniques used to interpret the data are detailed.

2.3.1 Sheath Effects

The collection area of a Langmuir probe is approximately equal to the area of the sheath. For an unbiased probe the sheath thickness can be assumed to be approximately equal to the Debye length which is defined to be

$$\lambda_D = \sqrt{\frac{\epsilon_0 T_e}{ne^2}} \tag{2.26}$$

In Basil, $\lambda_D \sim 5 \times 10^{-6}$m, while the smallest Langmuir probe has a radius of $a = 1.5 \times 10^{-4}$m, which is much larger than the sheath of an unbiased probe.

However, the Debye length can be an underestimate of the sheath thickness for a probe with a large negative applied bias. When a large negative bias is applied to the probe, electrons are expelled from a larger region due to the sheath. An estimate of the sheath

thickness can be determined from the cylindrical Child-Langmuir relation, together with the Bohm current. The cylindrical Child-Langmuir law is

$$\frac{i}{l} = \frac{8\sqrt{2}\pi\epsilon_0}{9}\sqrt{\frac{e}{m}}\frac{V^{\frac{3}{2}}}{a\beta^2} \tag{2.27}$$

where β is a constant proportional to a/b, the ratio of the probe and sheath radii, and l is the probe length. V is the voltage across the sheath and i is the ion current drawn by the probe. The ion flux at the sheath edge can be determined from the ion acoustic velocity (assuming that the Bohm criterion holds exactly).

$$j = \frac{i}{2\pi bl} = e0.6n_0\sqrt{\frac{kT_e}{m}} \tag{2.28}$$

Equating equations 2.27 and 2.28 gives:

$$b\beta^2 \equiv \frac{1.05}{a}\lambda_D^2\eta^{\frac{3}{2}} \tag{2.29}$$

Where η is defined, in terms of the probe bias V_B and the plasma potential V_P, as

$$\eta = \frac{e(V_P - V_B)}{kT_e} \tag{2.30}$$

For cylindrical and spherical probes which have $b/a < 3$, β can be approximated by b/a [76]. Using this approximation for β and typical plasma conditions for Basil, the sheath thickness can be as large as

$$\frac{b}{a} = 0.3 \tag{2.31}$$

which makes it important to include the sheath thickness in the analysis.

2.3.2 Magnetic Field Effects

There is little effect on Langmuir probes due to the applied magnetic field when the dimensions of the probe are much smaller than the Larmor radius of the collected species. Ions have a relatively large mass and thus large Larmor radii, so there is no effect on the ion current contribution to the probe current. Once the bias of the probe become small or positive, the probe collects low energy electrons which have a small Larmor radius. The Larmor radius is given by

$$r_L = \frac{mv_\perp}{|q|B} \tag{2.32}$$

For electrons to have a Larmor radii of the same size as the probe diameter, 0.1 mm, at the low field of 0.15T, they need an energy less than 4eV. Room temperature ions with an energy of approximately 0.025eV have a Larmor radii of 1mm at the same field.

Electrons with Larmor radii smaller than the dimensions of the probe can only be collected through diffusion across the field lines or from flux tubes intersecting the probe. It has been shown [61, 81] that the electron saturation current is reduced by a factor,

$$s = 16\lambda_{ei}\left(\frac{D\perp}{D\parallel}\right)^{\frac{1}{2}}\frac{\left(1+\frac{T_i}{T_e}\right)}{2\pi a} \tag{2.33}$$

Where λ_{ei} is the mean free path for collisions, ω_{ce} the electron cyclotron frequency, ν_{ei} the electron ion collision rate, $D_{||} = \frac{T_e}{m_e\nu_{ei}}$ the diffusion coefficient along the magnetic field lines, and $D_\perp = D_{||}\left(1+\frac{\omega_{ce}^2}{\nu_{ei}^2}\right)$ is the diffusion coefficient across the magnetic field

lines

For a typical argon plasma in Basil the reduction in electron saturation current is in the order of 0.05.

An important consideration for temperature measurements is the effect of the plasma potential on the probe current, particularly at small probe biases. As the plasma potential was not measured in Basil, electron temperatures were always measured in the region where the probe bias is less than the floating potential. It has been verified experimentally [109] that for this condition there is no distortion of the probe characteristic. This is because the electrons have no positive drift towards the probe relative to the ions. Thus, the magnetic field has little or no effect on the plasma parameters measured in Basil with a Langmuir probe.

2.3.3 RF Field Effects

The main disadvantage of using a Langmuir probe to measure the electron temperature in a plasma produced with rf power is the distortion of the probe characteristics in the region near the floating potential, where the temperature of the bulk electrons is usually measured. If the rf fluctuations are small enough that the probe current does not leave the exponential region of the Maxwellian distribution then averaging through filtering will give an undistorted probe characteristic.

Many techniques aimed at making the probe bias follow the rf fluctuations, and thus give the correct dc characteristics, have been suggested. One method [108] involves capacitively coupling the probe to the plasma, and making the probe circuit impedance at the rf frequency very large compared to the sheath impedance. This forces the probe bias

to follow the rf fluctuations and greatly reduces the rf fluctuation across the probe sheath.

The best method of increasing the impedance of the probe at the rf frequency is with self resonant inductors near the probe tip. The conflicting requirements of small inductor size and high plasma densities rendered this technique impossible in Basil. Another method used, by Paranjpe et al[95], to increase the probe impedance at the rf frequency, was to place a tuned circuit immediately outside the probe shaft. This technique was also attempted in Basil, however no difference in the probe characteristics were observed. The effectiveness was reduced by the relatively large capacitance of the probe shaft, which was by necessity constructed of a 30cm length of $\frac{1}{4}$ inch stainless steel tubing.

Increasing the capacitive coupling of the probe to the plasma can be done by making the radius of the insulated conductor section of the probe tip as large as possible, without being so large as to disturb the plasma [95]. This can also be done by using an electrode on the outside of the insulated probe tip coupled to the probe through a small capacitor. In Basil a small copper collar that fits tightly into the insulated probe tip was used, as shown in figure 2.12.

To circumvent any signal distortion due to rf effects, the electron temperature was determined from the negative voltage region of the probe characteristic. In any case the distortion due to the rf should be relatively small as the probe traces do not show features resembling the low energy drifting Maxwellian normally attributed to rf interference [60, 81]

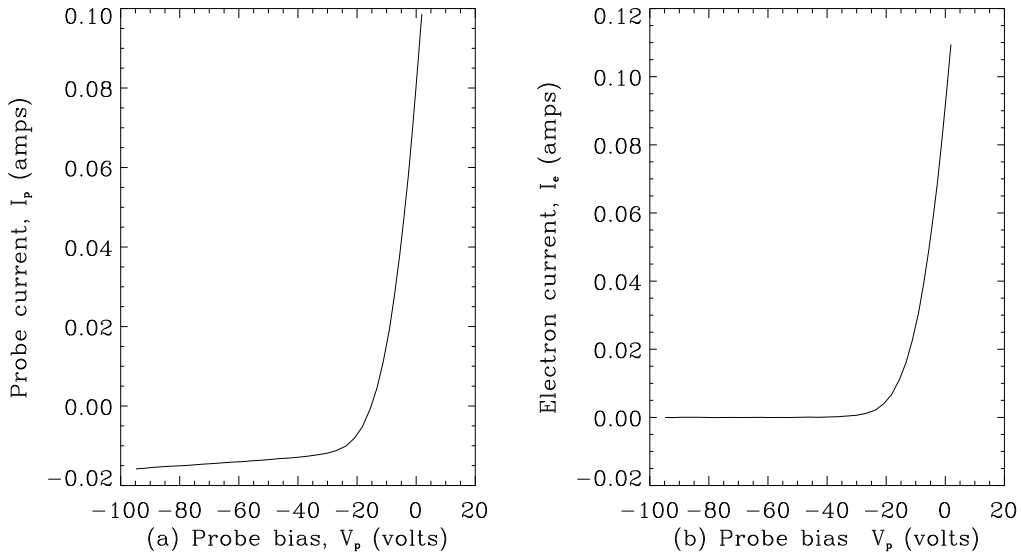

Figure 2.13: *(a) The total current to the Langmuir probe. (b) the electron current after ion current is subtracted.*

2.3.4 Probe Data Analysis

The first step in analysing the Langmuir probe data is to obtain an electron temperature. If the probe is biased negatively with respect to the plasma potential then the electron current measured with the probe, for non-drifting Maxwellian electrons, will be

$$I_e(V_p) = I_e^* \exp(\frac{-e(V_s - V_p)}{T_e}) \tag{2.34}$$

Where V_p is the probe bias, V_s is the plasma potential (so $V_s - V_p$ is the voltage across the probe sheath), T_e is the electron temperature, and I_e^* is the electron saturation current. The electron current is obtained by subtracting the ion current from the total probe current. In the simplest case the ion current saturates at large negative bias voltages, and this saturation current can then be subtracted from the total probe current to leave the

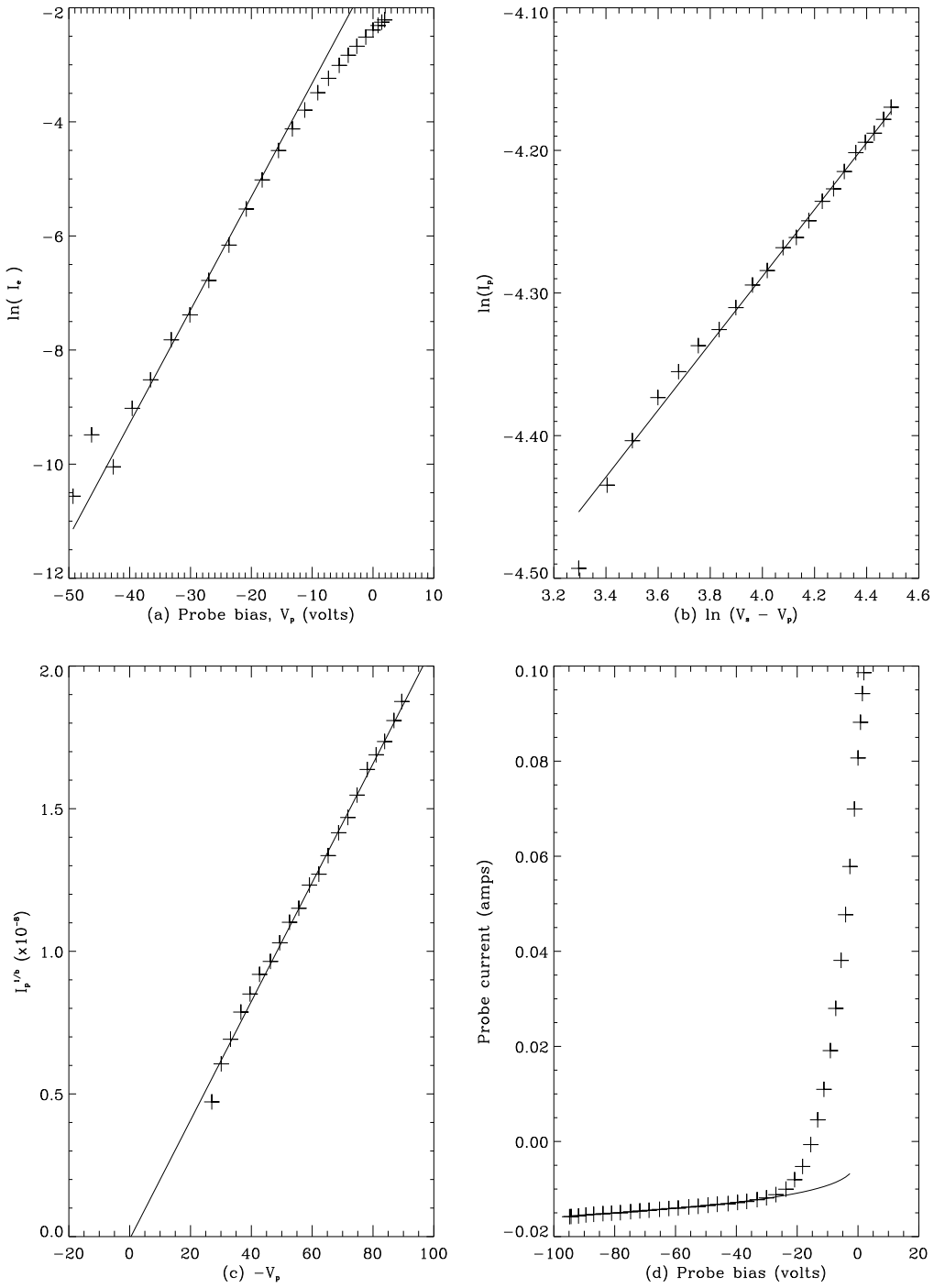

Figure 2.14: *Analysis method for the data in figure 2.13. From left to right, (a) Electron temperature, (b) first estimate of b, (c) first estimate of plasma potential, (d) fitted current. Raw data is marked with crosses and fitted curves are solid lines.*

electron current. In practice however large bias voltages cause the probe sheath to expand thus increasing the collection area of the probe. As a result the probe current continues to increase without saturating. Typically in Basil the ion current increases linearly with bias voltage, hence to obtain the electron current a straight line is fitted to the ion current at large bias voltages and this is subtracted from the total probe current (see figure 2.13). From equation 2.34 the electron temperature can be obtained from the inverse slope of the log of the electron current versus the probe bias (see figure 2.14(a)).

For the case in which the sheath radius is much smaller than the probe radius the ion saturation current at a large negative bias can be used to determine the plasma density, using Bohm's criterion. However, in Basil the sheath radius is a non-negligible fraction of the probe radius and a more complex technique must be used to determine the plasma density. Following the method derived by Steinbruchel [104] the ion current to the probe, I_i, is given by the equation

$$I_i = eN_iA\left(\frac{\epsilon_o kTe}{2\pi m_i}\right)^{1/2} i_i \tag{2.35}$$

where N_i is the ion density in the bulk plasma, m_i is the ion mass and i_i is a dimensionless correction factor dependent on a/λ_D (probe radius/Debye length). Steichbruchel determines an equation for i_i which corresponds to numerical results obtained by Laframboise [74] in modelling cylindrical probes

$$i_i(X) = a(-X)^b \tag{2.36}$$

where a and b are fitting constants and $X = e(V_p - V_s)/kT_e$, is the normalised potential across the probe sheath.

The fitting parameter a varies very little over the Basil parameter range and is taken to be 1.15 for all cases. Parameter b is then found using an iterative process. The first estimate, b_1, is determined from the slope of $\ln(I_i)$ versus $\ln(-V_p)$, as in figure 2.14 (b). This assumes that $-V_p \approx V_s - V_p$, which is true for large enough values of $-V_p$. Then a first approximate value for the plasma potential V_{s1} is found from the intercept of I_i^{1/b_1} versus $-V_p$ (see figure 2.14 (c)). A second value value of b, b_2, can be determined from the slope of $\ln(I_i)$ versus $V_{s1} - V_p$, and the process can be repeated until convergence is obtained. In practice only two iterations are required.

Once values for a and b are determined the plasma density can be found using the slope of $I_i^{1/b}$ versus $-V_p$, using an equation derived from equations 2.35 and 2.36

$$N_i = \left(-\frac{\delta I_i^{1/b}}{\delta V_p} \right)^b (aA)^{-1} (2\pi m_i)^{1/2} e^{-b-1} (kT_e)^{b-1/2} \tag{2.37}$$

Figure 2.14 (d) shows the fitted ion current calculated from equation 2.35 using the plasma density determined in equation 2.37, plotted together with the experimental data.

2.4 Hybrid Combiners

The transmission line transformer in figure 2.15 is very similar to transformers described by Ruthroff [100] and is thus referred to as the Ruthroff hybrid combiner. It is used to separate the common mode and difference mode signals of magnetic probes, differen-

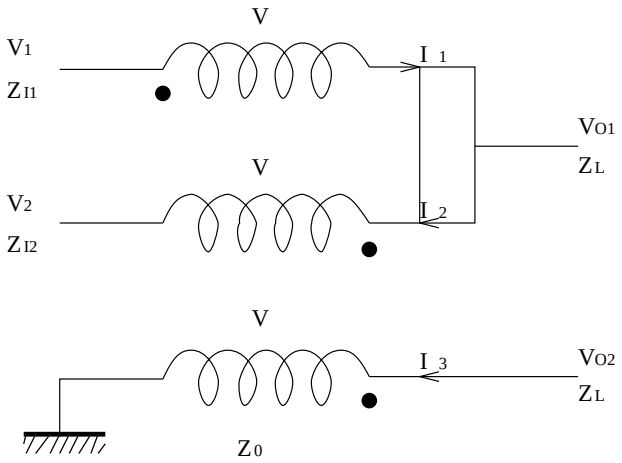

Figure 2.15: *Circuit diagram of a hybrid combiner.*

tial voltage probes, or any rf system when common mode pickup is likely to corrupt a differential voltage measurement. It is constructed with a tri-filar winding on a small toroidal ferrite. Treating the hybrid combiner as a transformer, ignoring transmission line effects [11] and using Kirchoff's laws to analyse the circuit in figure 2.15 gives the following equations

$$V_1 - V_2 = 2V \tag{2.38}$$

$$V_{02} - V = 0 \tag{2.39}$$

$$V_{01} - V_1 + V = 0 \tag{2.40}$$

Using these equations for given input signals, V_1 and V_2, expressions for the output signals can be found

$$V_{01} = \frac{V_1 + V_2}{2} \tag{2.41}$$

$$V_{02} = \frac{V_1 - V_2}{2} \tag{2.42}$$

Since the windings are tri-filar the self inductances and mutual inductances are equal, giving

$$V = j\omega L(i_1 + i_2 + i_3) \tag{2.43}$$

where L is the self inductance.

This circuit has the property that V_1 and V_2 are isolated; signal fed in V_1 appear at V_{01} and V_{02}, but not at V_2 and vice versa. A necessary condition for isolation is that

$$\omega L \gg Z_L \& Z_0 \tag{2.44}$$

where Z_0 is the characteristic impedance of the tri-filar transmission line and Z_L is the load impedance. Thus

$$i_1 + i_2 + i_3 = 0 \tag{2.45}$$

When a hybrid combiner is used for a probe it is important to terminate the transmission line from the probe in its characteristic impedance. The input impedance of the hybrid combiner can be calculated from the above equations and Ohm's law.

$$Z_{I1} = 2Z_L \tag{2.46}$$

$$Z_{I2} = 2Z_L \tag{2.47}$$

Thus, if 50Ω coaxial cable determines the system characteristic impedance, then 50Ω needs to be placed in parallel with the output cable (i.e. $Z_L = 25\Omega$ and $Z_I = 50\Omega$)

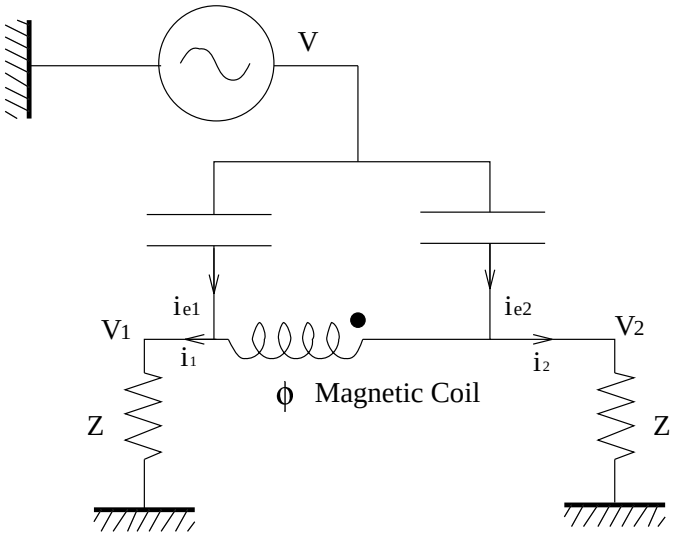

Figure 2.16: *Equivalent circuit of a magnetic probe.*

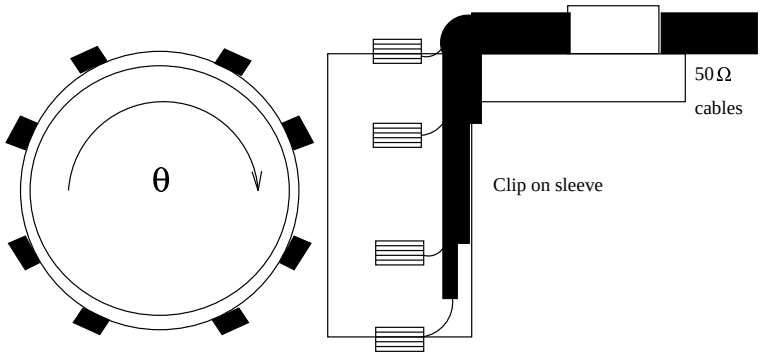

Figure 2.17: *End view, and side view of the azimuthal magnetic probe array.*

matching the input cable impedance.

2.5 Magnetic Probes

The magnetic probes used to measure the magnetic wavefields in the plasma are simple inductive pickup coils. The coils range in diameter from 3mm for probes in the plasma to 5mm for probes outside the vacuum vessel. It has been found that it is easier and

Calibration factor (Gauss V_{rms}^{-1})					
Radial Probe			Longitudinal Probe		
r	θ	z	r	θ	z
11	7.9	8.9	46	19	6

Table 2.5: *Calibration for the radial and longitudinal 3 component magnetic probes at 7MHz.*

more reliable to use simple coils and separate the magnetic and electric pickup with a hybrid combiner than to use more complicated probe techniques such as centre tapping or shielding. To see how this is achieved consider the voltage signals V_1 and V_2 in the equivalent circuit of a probe in figure 2.16.

$$V_1 = \phi_1 - \frac{j\omega L}{Z} i_1 + i_{e1} Z \tag{2.48}$$

$$V_2 = \phi_2 - \frac{j\omega L}{Z} i_2 + i_{e2} Z \tag{2.49}$$

where $i_{e1}Z$ and $i_{e2}Z$ are the capacitively coupled signals in each arm due to a stray electric field. When the probe is small and shield coaxial cable, or tight bifilar windings, are used then $i_{e1} \equiv i_{e2}$. ϕ_1 and ϕ_2 are the inductively coupled signals due to the oscillating magnetic field. Because of the symmetry of the system, accomplished by using identical coaxial cable for each side of the probe, the magnetic signal will be of equal amplitude and 180^0 out of phase, so that $\phi_1 = -\phi_2$, and $i_{e1} = i_{e2}$. Substituting V_1 and V_2 from equations 2.48 and 2.49 into the inputs of a hybrid combiner (usually via coaxial cable or twisted pair transmission line, Z) equations 2.41 and 2.42 give the output signals of the

hybrid combiner.

$$V_{O1} = i_e Z \tag{2.50}$$

$$V_{O2} = \phi + \frac{j\omega L}{Z} i \tag{2.51}$$

where

$$i_e = i_{e1} + i_{e2} \tag{2.52}$$

$$\phi = \phi_1 - \phi_2 \tag{2.53}$$

Thus, the hybrid combiner can be used to separate the signals into electric and magnetic components. This works very well experimentally, with less than 5% cross talk between the two signals at 5MHz and allows the pickup current to be measured directly.

There are three main arrangements of magnetic probes in this experiment. The first is the azimuthal array of magnetic probes shown in figure 2.17. This consists of 8 coils attached around a sleeve which can be fitted over the Pyrex vacuum vessel to permit axial measurement of the azimuthal magnetic field profile. The probe array was calibrated by placing it inside two coaxial conductors 90cm long attached to a conducting end plate. (the inside conductor is the same size as the Pyrex tube). By measuring the current in the centre conductor the magnetic field can be calculated and a calibration factor for the probe determined.

The other arrangements are three component probes which are inserted into the plasma, a radial probe placed 20cm axially from the antenna, and a longitudinal probe inserted from the end plate. They consist of three coils wound on top of each other in orthogonal planes to minimise mutual inductance. These probes are calibrated using a Helmholtz coil

(see calibration factors in table 2.5), and the measured cross talk between components of the probe was less than 5%.

2.6 Data Collection and Analysis

To facilitate the collection of rf signals with digitisers of a maximum digitisation speed of 40kHz, three 8 channel 0.4-40MHz phase and amplitude detectors were used [43]. The detection circuits used in these devices are quadrature interferometers that compare the data signal with a reference rf signal and produce two outputs, $A\,sin\theta$ and $A\,cos\theta$, where θ is the phase difference between the reference and data signals and A is the amplitude of the data signal. Reference signals are obtained from the rf control system of the transmitter.

The data is digitised with CAMAC controlled LeCroy 8212A 16 and 32 channel digitizers with a clock rate of 5kHz, which allows all 48 channels to be collected simultaneously. Digitization rates of 40kHz can be obtained with these digitizers with limited channels. A LeCroy 2264 digitizer with a clock rate of 2MHz was used for digitizing Langmuir probe signals for detailed analysis. To trigger the rf system and to control the voltage on the Langmuir probes a LeCroy 8601 waveform generator was used. Handling of the data and control of the CAMAC create is done with MDS software on a VAX/VMS 4000/60 workstation.

The raw data is analysed and displayed using the programming language IDL (Interactive Data Language). IDL programmes calibrate the raw data to obtain amplitude and phase with respect to the reference signal and correct phase errors in the detectors. Many programmes have been written to allow easy analysis of the large amounts of data that

can be taken simultaneously (up to 24 rf signals). The programs used to collect, analyse, and manage the data are discussed in appendix A. Because of the large amounts of data obtained, after analysis, the raw data is archived on the Australian National Universities large data storage facility (the StorageTek robotic tape silo at the ANU Supercomputer faculty), which allows easy access for re-analysis.